Mesoscale Boundaries from differential surface heating

The general paradigm here:

A difference in surface characteristics

↓

Spatial differences in surface heating

↓

Horizontal ∇T (or buoyancy)

↓

Acceleration of $\vec{V}$, convective circulations.

Whatever the exact cause of the spatial differences in surface heating, end result is a thermally direct circulation that acts to equilibrate surface temperature difference.

Thermally direct convective cell.

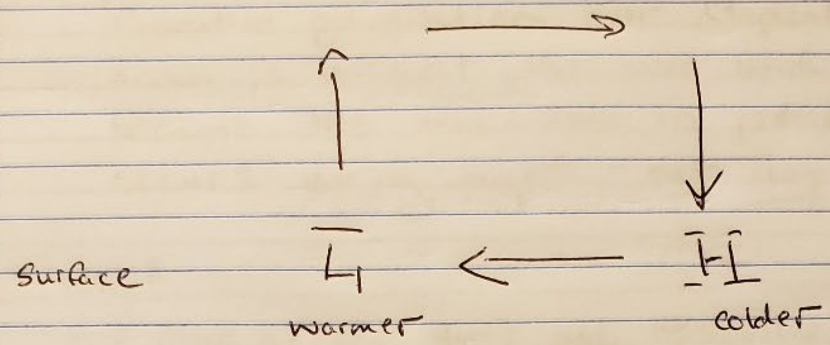

Why is this important for mesoscale?

- The surface gradient forced diurnal circulations provide a local mechanism for lift through PBL

- Rising air may form convective clouds which may transition to deep convection if reach LFC.

⇒ Basically a principal convective triggering mechanism!

Almost <u>always</u> tied to diurnal cycle of solar heating during day, cooling at night, so that explains the well observed diurnal maximum in convective precip <u>over</u> <u>land</u>.

* Important Aside!

Convective precipitation over (tropical) ocean is different than over land because the maximum in precip occurs during night - <u>not</u> <u>day</u>!

Why?

→ Over ocean there are basically no surface inhomogeneities. So <u>only thing</u> that makes the atmosphere change its stability is radiational heating and cooling. Therefore radiational cooling at night over makes the atmosphere less stable and more susceptible to convection.

... More on this point in tropical meteorology.

Sea and land breezes

- Caused by differences in heat capacities of water to land
  - Land: low specific heat capacity
    → heat, cool fast
  - Water: high specific heat capacity
    → heat, cool slow
- Most apparent when synoptic forcing is weak

$\boxed{\text{DAY}}$

Sea breeze
Onshore flow

$\boxed{\text{NIGHT}}$

Land breeze
offshore flow.

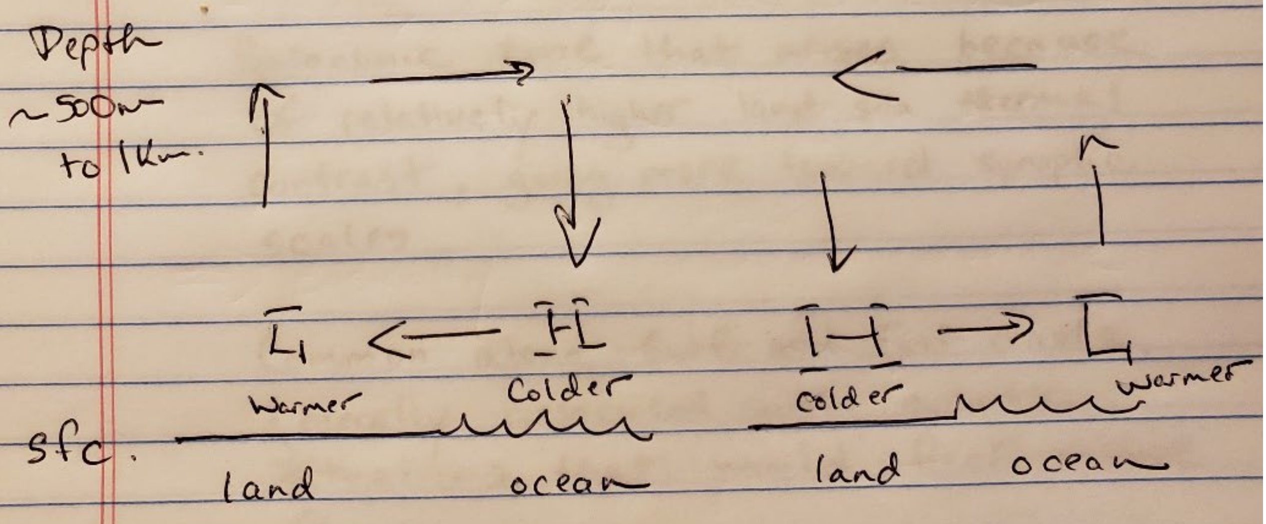

Sea breeze on order of 5-10 $m\,s^{-1}$

⇒ Classic CONUS example: Florida!

The Adequacy of the Hydrostatic Assumption in Sea Breeze Modeling over Flat Terrain

CHARLES L. MARTIN

Simpson Weather Associates, Charlottesville, VA 22901

ROGER A. PIELKE

Department of Atmospheric Science, Colorado State University, Fort Collins, 80523

(Manuscript received 15 December 1982, in final form 11 March 1983)

ABSTRACT

Using a linear analytic model and a nonlinear numerical model, the adequacy of the hydrostatic model is investigated for use in the simulation of sea and land breezes over flat terrain. Among the results it is found that for a given horizontal scale of heating, the hydrostatic assumption becomes less valid as the intensity of surface heating increases, and as the synoptic temperature lapse rate becomes less stable. The spatial scale at which the hydrostatic assumption fails is substantially smaller than suggested by Orlanski (1981). For sufficiently stable large-scale thermodynamic stratifications, for instance, aspect ratios of order unity can still produce nearly identical solutions, regardless of whether or not the hydrostatic assumption is used. The difference in the conclusions between our study and that of Orlanski is attributed to Orlanski's analyses of the characteristic wave equations in the free atmosphere, whereas in a sea-breeze simulation the requirement that vertical velocity at the ground is zero limits the magnitude of the vertical acceleration.

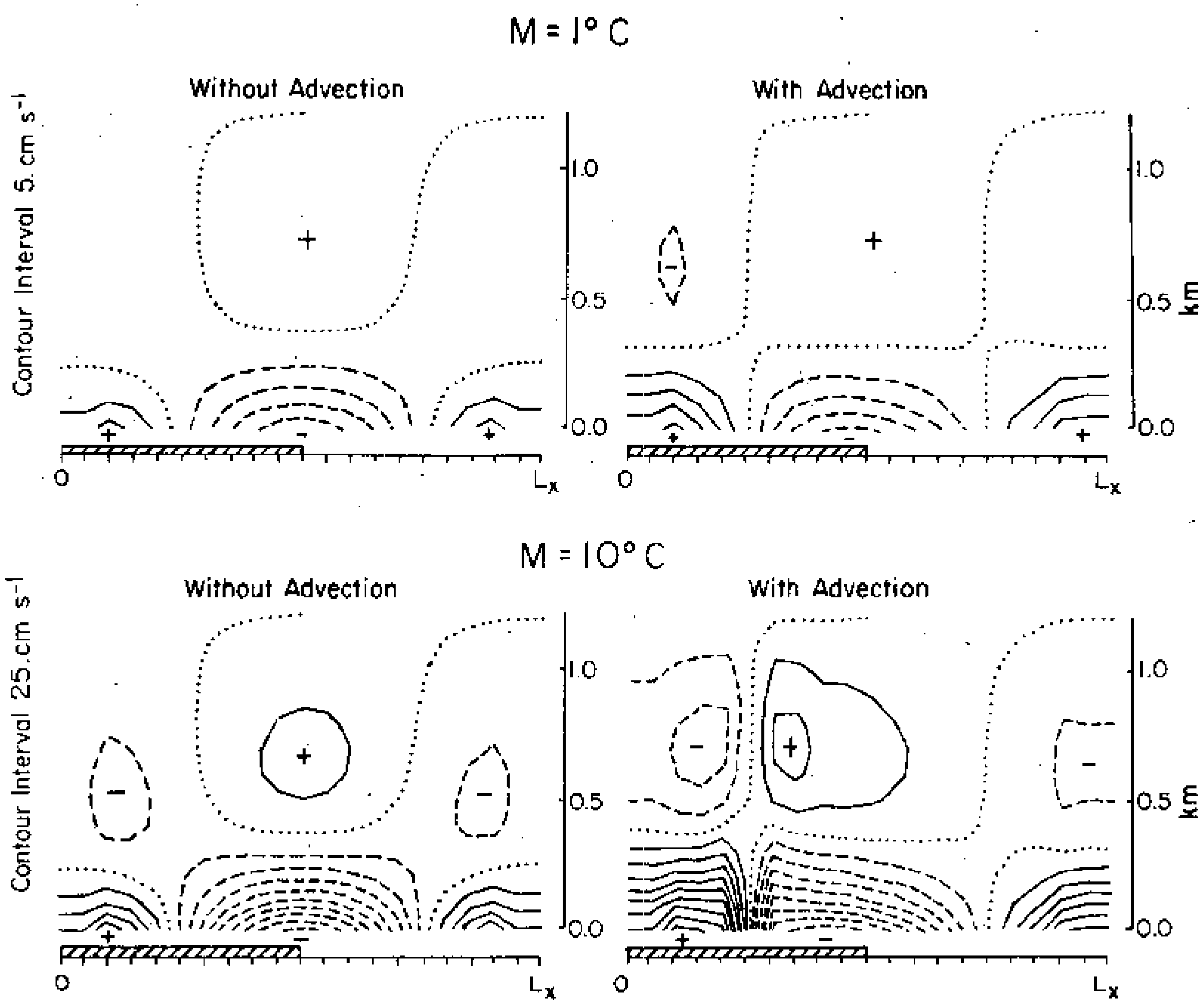

FIG. 6. The simulation of the sea breeze using the numerical analog of Defant's model with M = 1°C (top) and 10°C (bottom), without (left) and with nonlinear advection included.

Exactly as we have discussed before for fronts and dry lines, the non-linear effects on advection will cause air to form tighter ∇T, forming a sea-breeze front with local pressure minima!

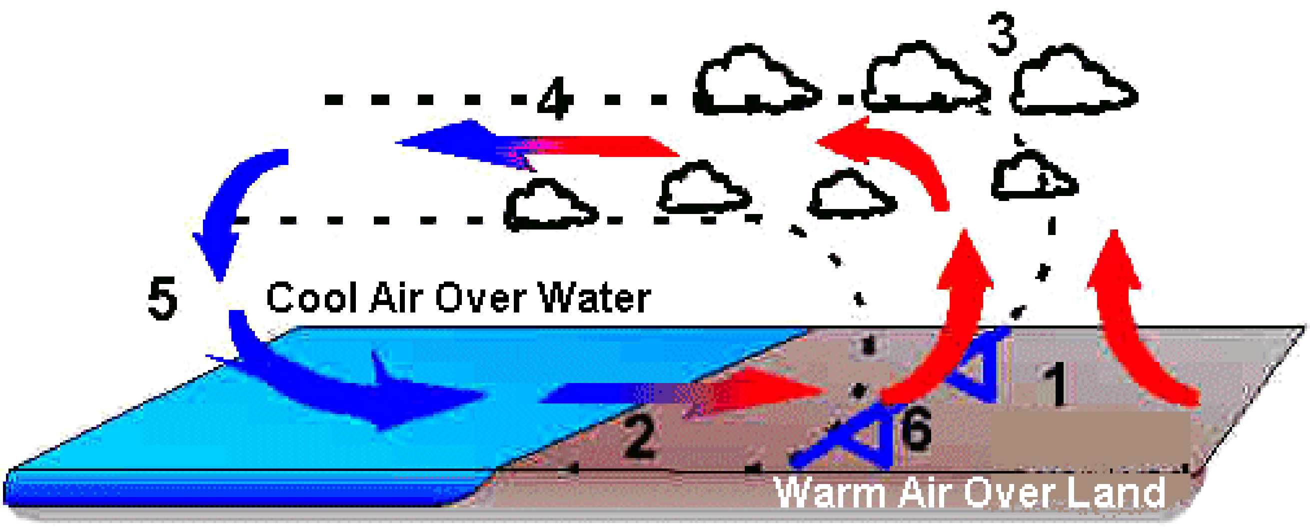

3
4
5
Cool Air Over Water
1
2
6
Warm Air Over Land

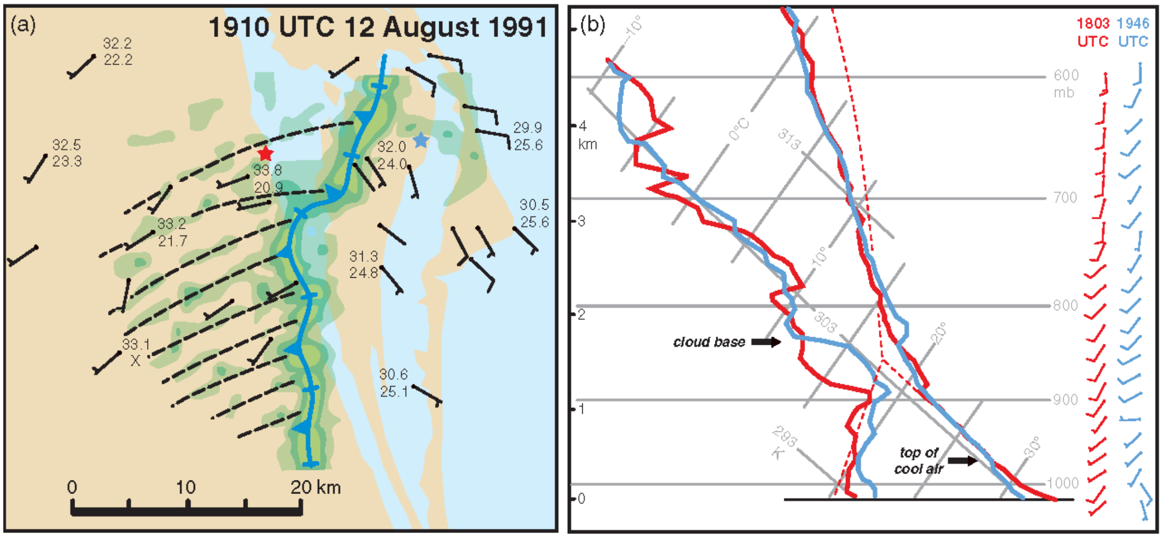

Figure 5.33 (a) Analysis of a sea-breeze front on the east coast of Florida on 12 August 1991 during the Convection and Precipitation/Electrification Experiment (CaPE). Station models display temperature and dewpoint in °C, and wind barbs in knots. Three levels of radar reflectivity are shaded; the thresholds are 0, 4, and 8 dBZ. The locations of updrafts associated with horizontal convective rolls are indicated with black dashed lines. (b) Soundings launched on opposite sides of the sea-breeze front depicted in (a). The blue (red) sounding was obtained in the cool (warm) air mass at the location of the blue (red) star in (a). The trajectory followed by a lifted inland parcel is also shown, as is the photogrammetrically determined cloud base. (Adapted from Wakimoto and Atkins [1994].)

Thunderstorms would tend to form at this boundary and then migrate inland and retreat toward shore.

Some deflection of the wind due to Coriolis force, friction!

Sea Breeze Front: North Carolina Example

EARLY MORNING

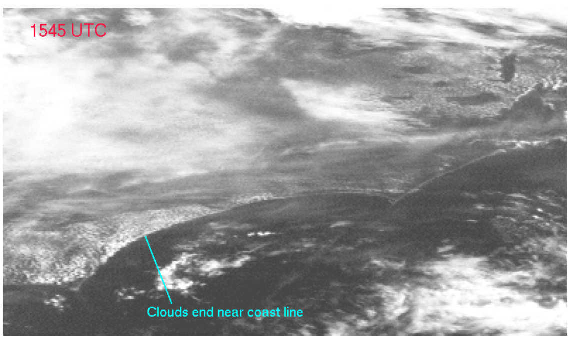

MID MORNING

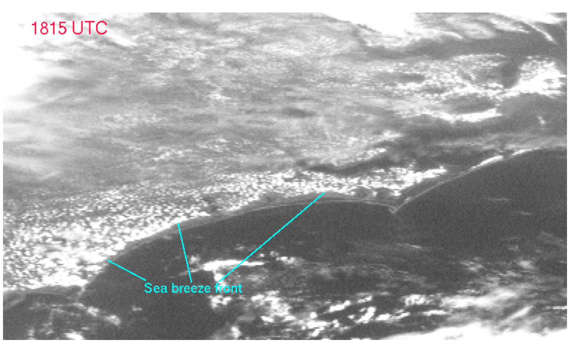

MID AFTERNOON

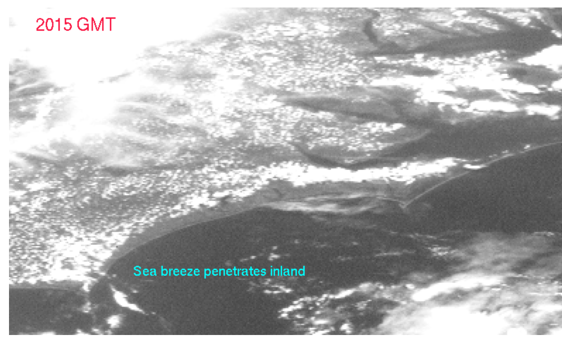

LATE AFTERNOON

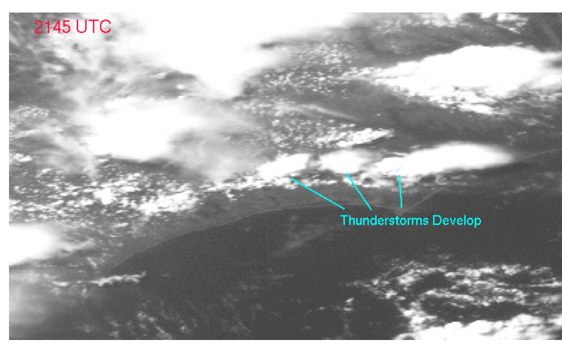

(University of Wisconsin)

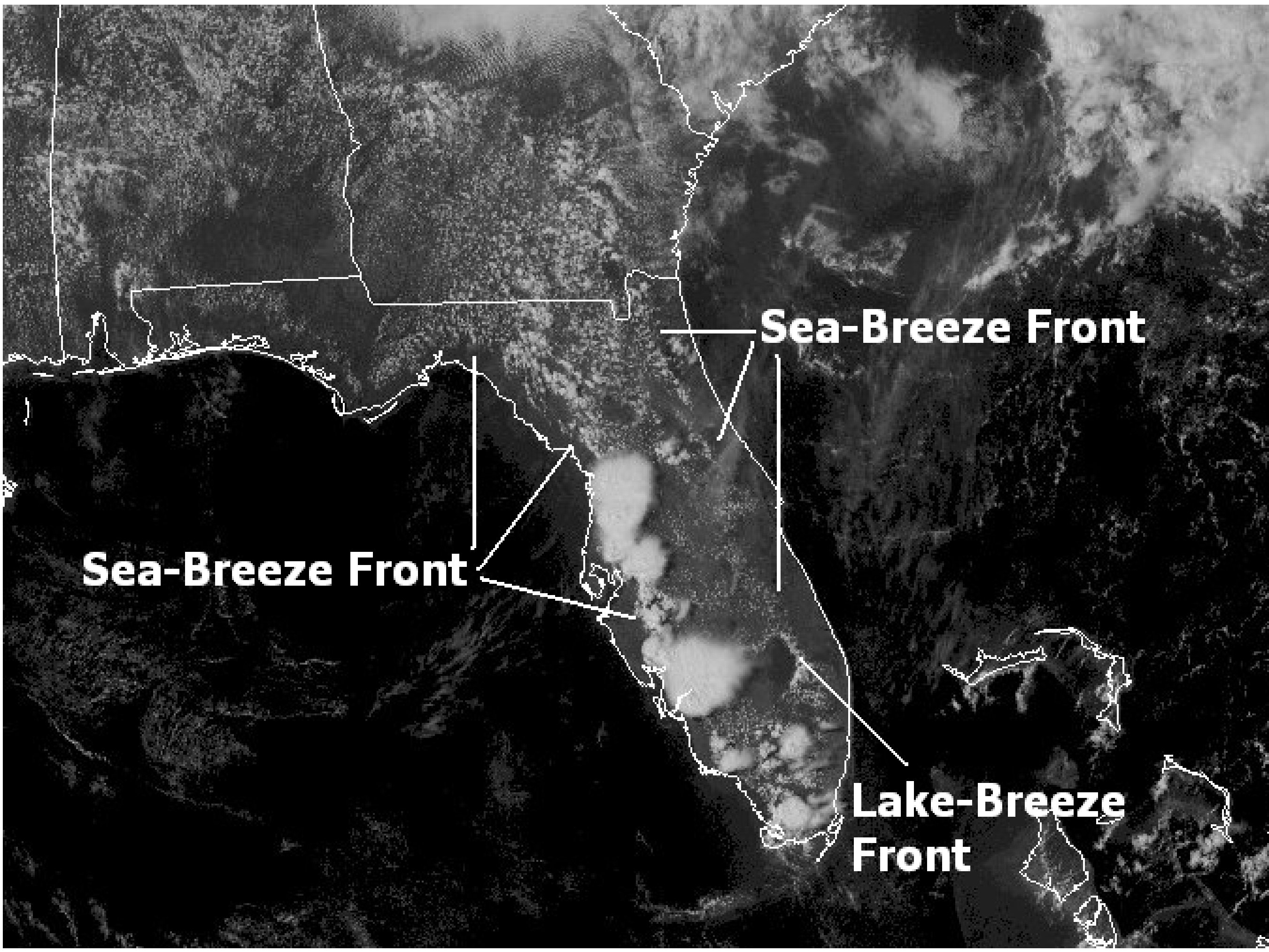
Sea-Breeze Front
Sea-Breeze Front
Lake-Breeze
Front

Coastal fronts

Baroclinic zone that arises because of relatively higher land sea thermal contrast, going more toward synoptic scales.

Common along Gulf and East coasts, generally associated with synoptic situations that would favor onshore flow

=> Can also be focal points for cyclogenesis, as discussed in WAF I

1800 UTC 13 March 1980

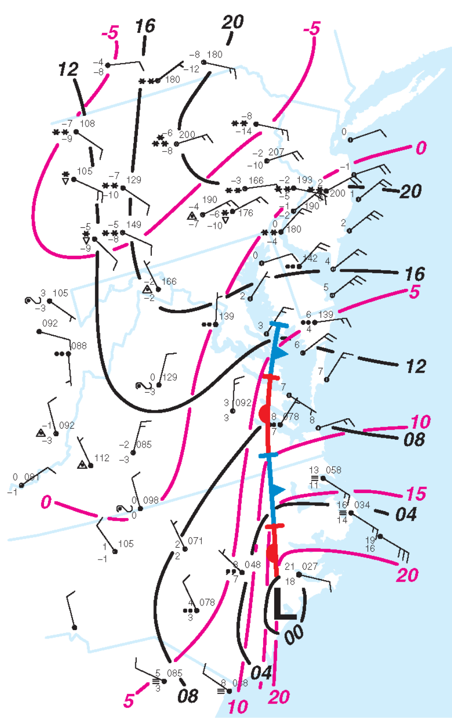

Figure 5.34 Analysis of a coastal front on 13 March 1980. Mean sea level pressure (mb; black contours; the leading '10' has been dropped) and temperature (°C; magenta contours) are analyzed. (Adapted from Bluestein [1993].)

Horizontal gradients in clouds, vegetation, soil moisture, or albedo.

Basically a surface gradient in <u>any</u> of these properties may trigger mesoscale circulations

Clouds: shading effects affect surface heating

→ Would have largest heating and upward motion ahead of (optically thick) deep clouds, and this is typically where θ_e would be locally maximized in a meso analysis.

* CAVEAT! Presents a BIG forecast challenge because how the convection evolves on a given day depends on cloud cover and where blow off of cirrus anvils would be creating shaded and sunny areas.

Can only figure that out in a "now cast" sense as storms evolve in real time.

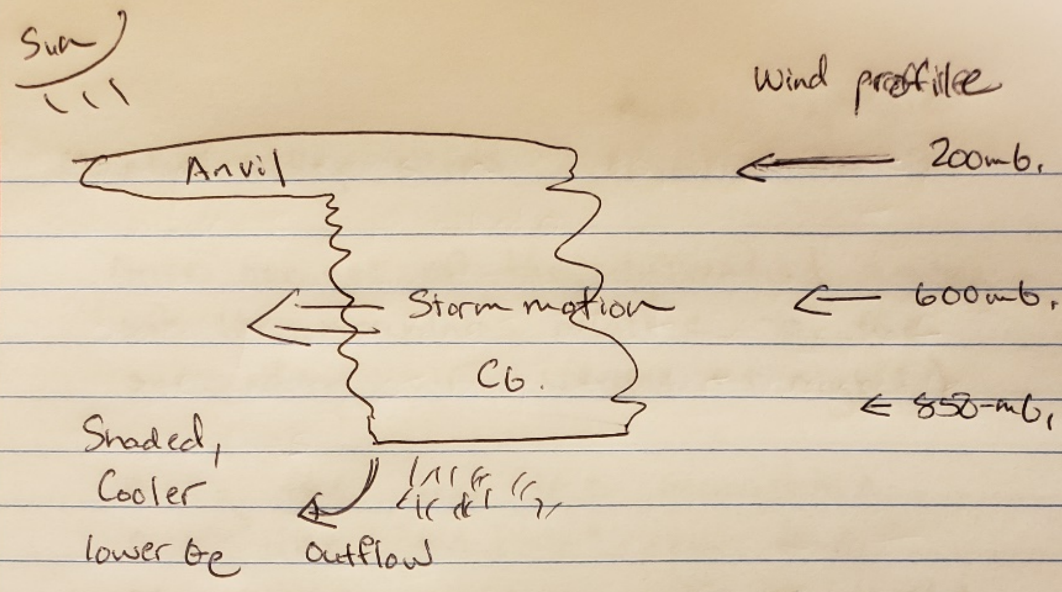

Cirrus anvils blow off <u>ahead</u> of storm
$\Rightarrow$ inhibited surface heating, lower θ_e
$\Rightarrow$ storm weakens!

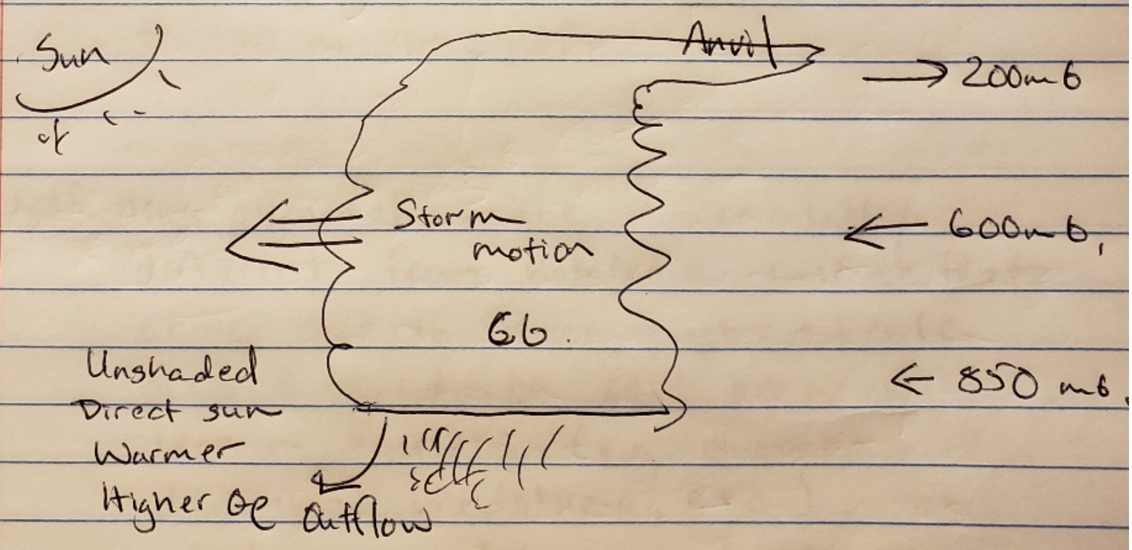

Cirrus anvils blow off behind or to sides of storm
$\Rightarrow$ enhanced surface heating, higher θ_e
$\Rightarrow$ Storm strengthens!

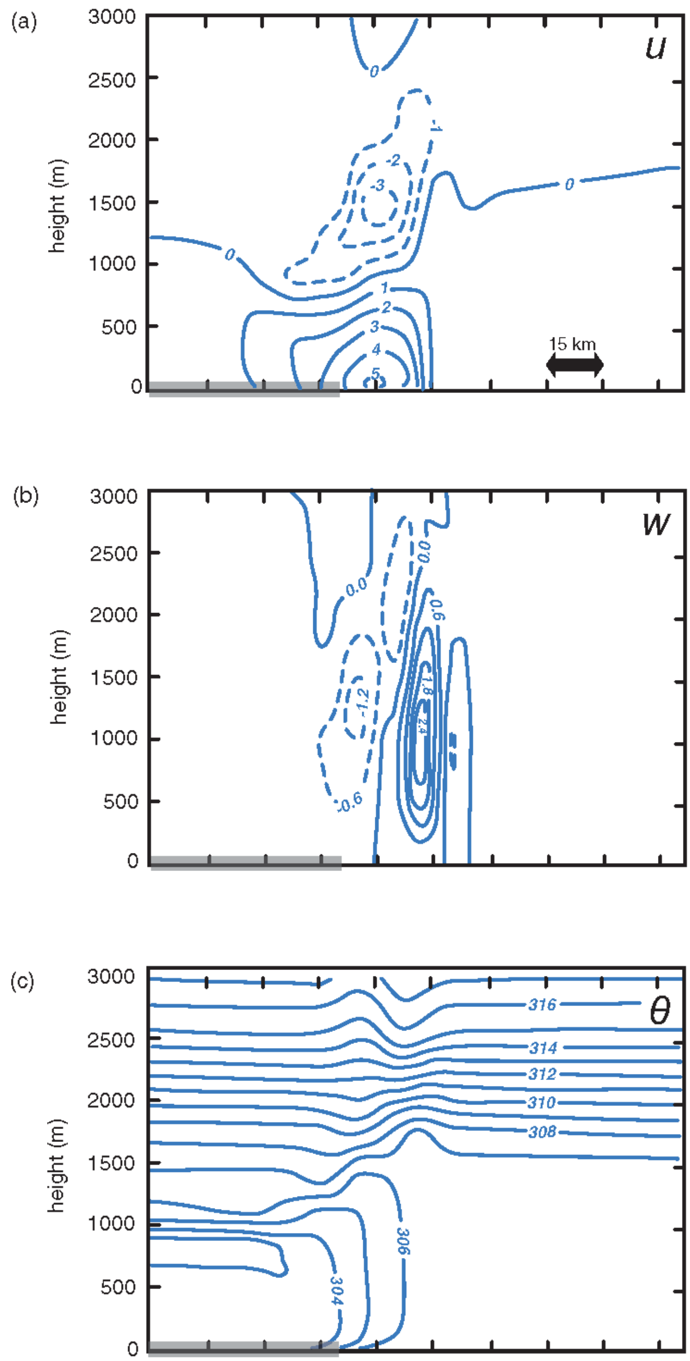

Figure 5.38 Idealized simulation of a mesoscale circulation produced by differential heating across the edge of a cloud deck. Vertical cross-sections of (a) u (m s^{-1}), (b) w (m s^{-1}), and (c) θ (K) are shown. The cloud layer spans the horizontal region indicated with the heavy, gray line. (Adapted from Segal *et al.* [1986].)

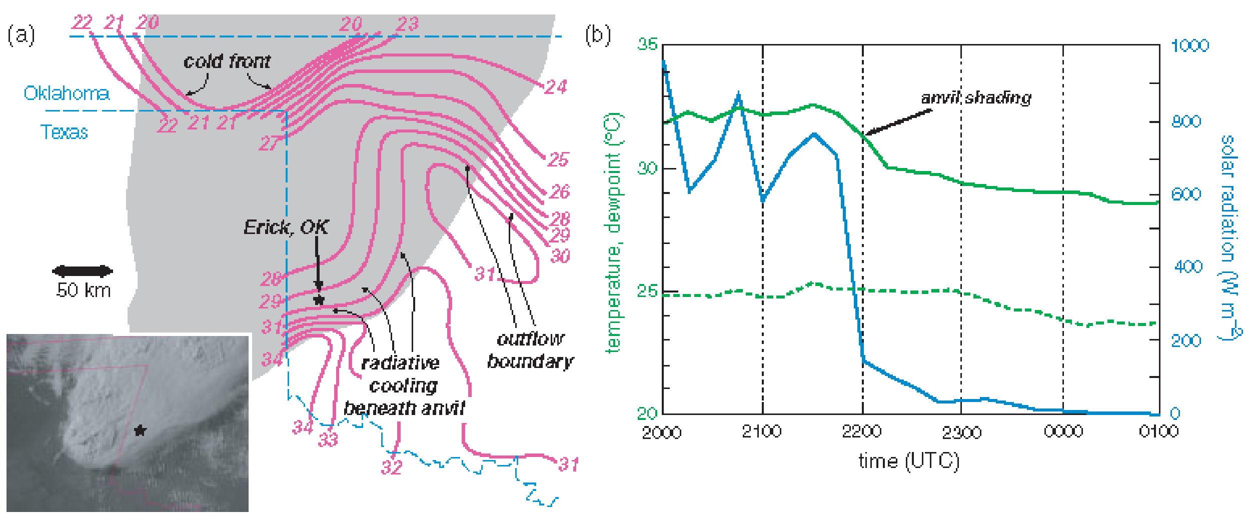

Figure 5.39 (a) Surface temperatures (contoured at 1°C intervals) at 2300 UTC 8 June 1995. The anvil canopy associated with a line of thunderstorms (see inset visible satellite image) is shaded gray. (b) Time series of temperature (solid green) and dewpoint (dashed green), both in °C, and solar radiation (solid blue), in W m^{-2}, from 2000 to 0100 UTC 8–9 June 1995 at Erick, OK (its location is indicated in [a]). (Adapted from Markowski *et al.* [1998].)

Convective Initiation at the Dryline: A Modeling Study

CONRAD L. ZIEGLER

NOAA/National Severe Storms Laboratory, Norman, Oklahoma

TSENGDAR J. LEE* AND ROGER A. PIELKE SR.

Department of Atmospheric Science, Colorado State University, Fort Collins, Colorado

(Manuscript received 25 April 1996, in final form 24 September 1996)

ABSTRACT

A nonhydrostatic, three-dimensional version of the Colorado State University Regional Atmospheric Modeling System (CSU-RAMS) is used to deduce the processes responsible for the formation of drylines and the subsequent initiation of deep, moist dryline convection. A range of cumuliform cloud types are explicitly simulated along drylines on 15, 16, and 26 May 1991 in accordance with observations.

In the simulations, narrow convergence bands along the dryline provide the lift to initiate deep moist convection. The thermally direct secondary convective boundary layer (CBL) circulations along the dryline are frontogenetic and solenoidally forced. Maximum updrafts reach 5 m s^{-1} and the bands are 3–9 km wide and 10–100 km or more in length. The updrafts penetrate and are decelerated by the overlying stable air above the CBL, reaching depths of about 2000 m in the cases studied. Moisture convergence along the mesoscale updraft bands destabilizes the local sounding to deep convection, while simultaneously decreasing the CIN to zero where storms subsequently develop. The lapse rates of vapor mixing ratio and potential temperature in the mesoscale updrafts are rather small, indicating that increases of the lifted condensation level (LCL) and level of free convection (LFC) due to mixing following the parcel motion are also small. Simulated convective clouds of all modes, including shallow forced cumulus and storms, develop in regions where the CIN ranges from zero up to the order of the peak kinetic energy of the boundary layer updraft and moisture is sufficiently deep to permit water saturation to develop in the boundary layer.

The findings suggest that classic cloud models may not adequately simulate the early development of dryline storms due to their use of thermal bubbles to initiate convection and their assumption of a horizontally homogeneous environment. In contrast, cautious optimism may be warranted in regard to operational numerical prediction of drylines and the threat of attendant deep convection with mesoscale models.

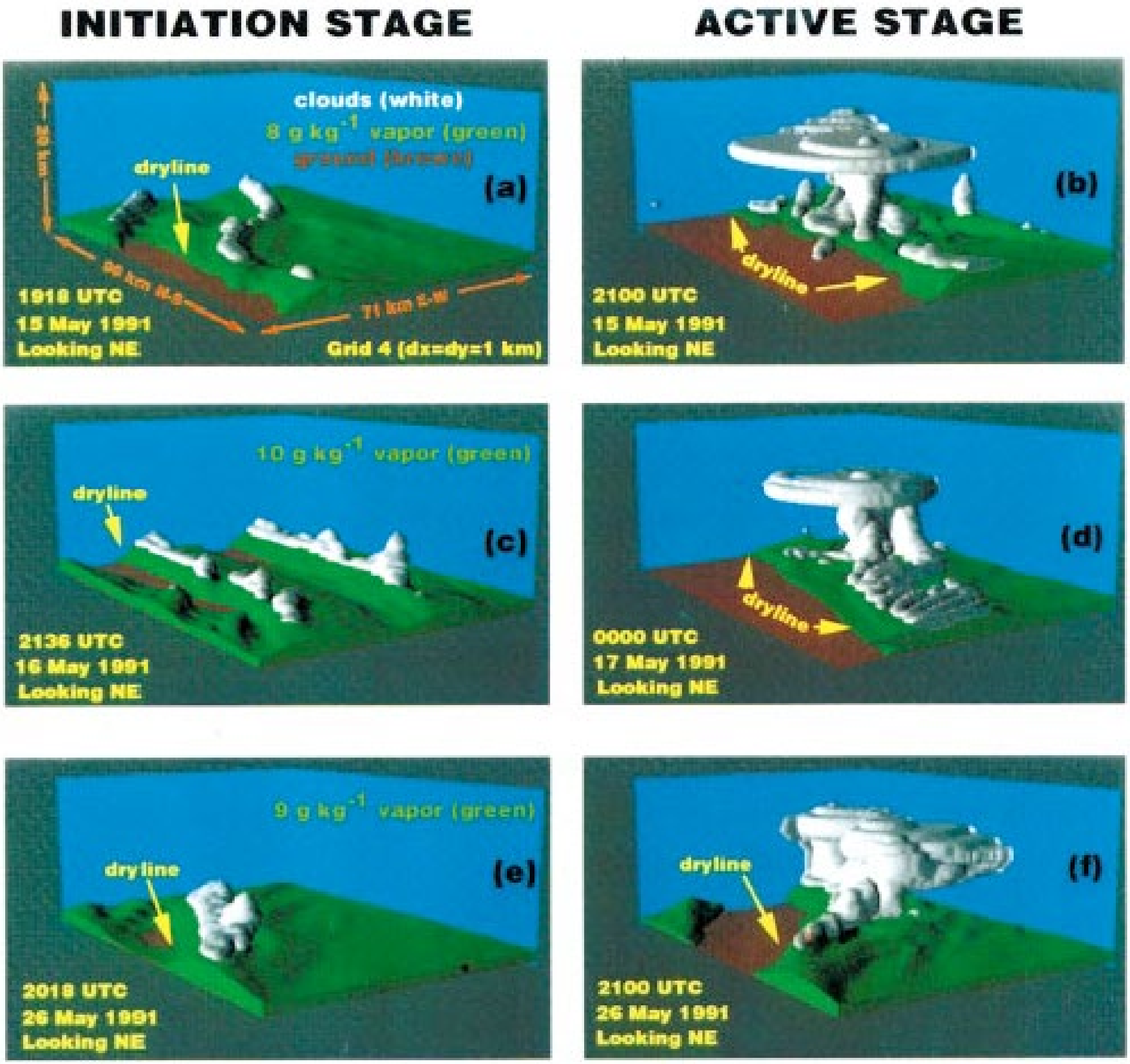

FIG. 19. Surfaces of cloud and constant vapor mixing ratios in perspective view on grid 4 at the initiation and active stages of simulated deep dryline convection. (a) 1918 UTC 15 May 1991; (b) 2100 UTC 15 May 1991; (c) 2136 UTC 16 May 1991; (d) 0000 UTC 17 May 1991; (e) 2018 UTC 26 May 1991; (f) 2100 UTC 26 May 1991. In panels (a) and (b), (c) and (d), and (e) and (f) the vapor mixing ratio surfaces have values of 8, 10, and 9 g kg^{-1}, respectively.

Second Edition

Mesoscale Meteorological Modeling

ROGER A. PIELKE SR.

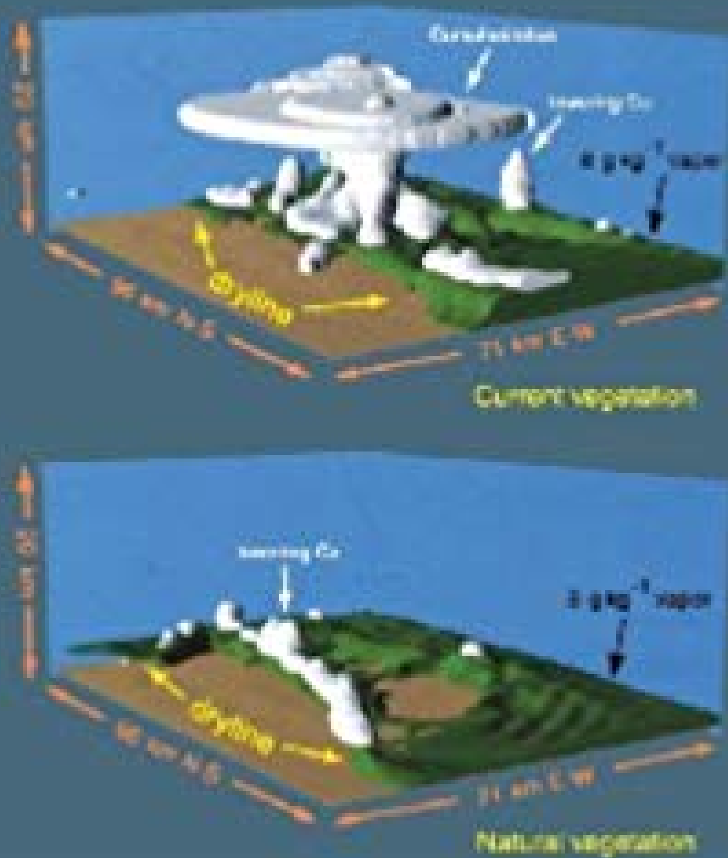

INTERNATIONAL GEOPHYSICS SERIES, VOLUME 78

Anabatic - upslope
Mountain valley winds   Katabatic - downslope

Arise because of the differential heating of the mountains relative to the surrounding air (reverse at night)

During the day the mountains act like "heaters" in the atmosphere, creating more positively buoyant air that is drawn up their slopes.

Peak speeds of 1-5 $m\,s^{-1}$

50-150 m in depth

Note These phenomena are fundamentally different from katabatic winds that arise due to more synoptic-scale pressure gradients that occur with terrain barriers. (e.g. chinooks, downslope windstorms, etc). These mainly worry during cool season

Refer back to WAF I . .

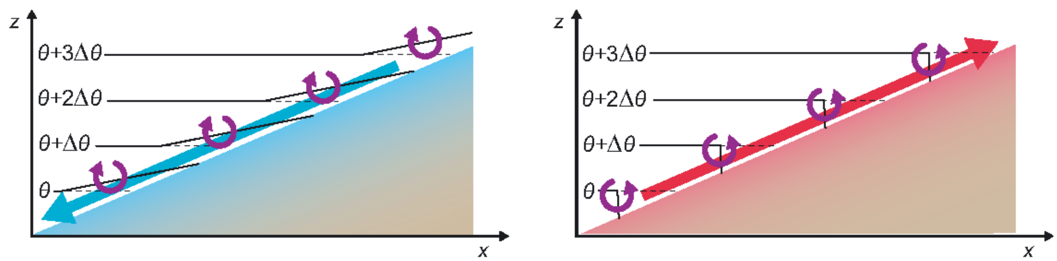

Figure 11.1 Illustration of the generation of (left) downslope and (right) upslope winds by the cooling and heating of sloped terrain, respectively. The thick solid black contours are isentropes that have been modified by surface cooling and heating, respectively. The dashed black lines are unmodified isentropes. The purple arrows indicate the sense of the horizontal vorticity production by the horizontal buoyancy gradient. The broad blue and red arrows indicate the sense of downslope and upslope flow along the surface, respectively, implied by the baroclinic horizontal vorticity generation.

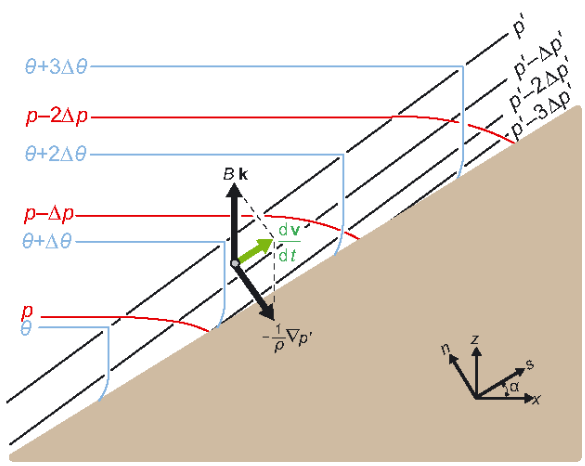

Figure 11.3 Force diagram in the case of a daytime, thermally driven upslope flow in which the depth of the temperature perturbation increases in the upslope direction. Isentropes are blue, perturbation pressure contours are black, and full pressure contours are red. The perturbation pressure gradient gives a small positive contribution to upslope acceleration in this case. Perpendicular to the slope, the flow is quasi-hydrostatically balanced. In the special case of along-slope thermal homogeneity, the perturbation pressure contours would be parallel to the slope and the perturbation pressure gradient would be exactly perpendicular to the terrain. (Adapted from Haiden [2003].)

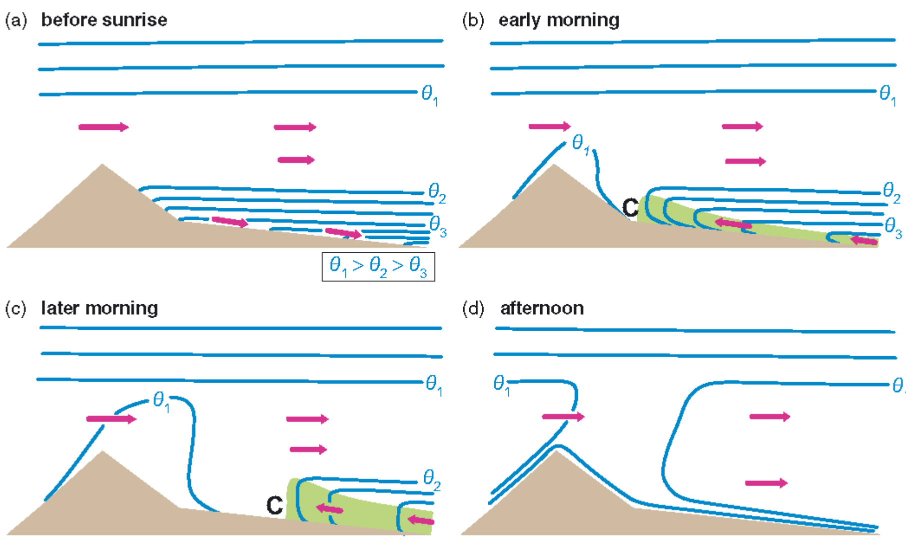

Figure 11.4 Evolution of potential temperature and winds from (a) before sunrise to (b) early morning to (c) late morning to (d) afternoon as a result of the development of a thermally forced anabatic wind (the previous night's katabatic wind is evident in [a]). An ambient wind also is present, blowing from left to right. The shaded region indicates a shallow mixed layer that contains the upslope flow, and the C at the upwind edge indicates the convergence zone. (Adapted from Banta [1990].)

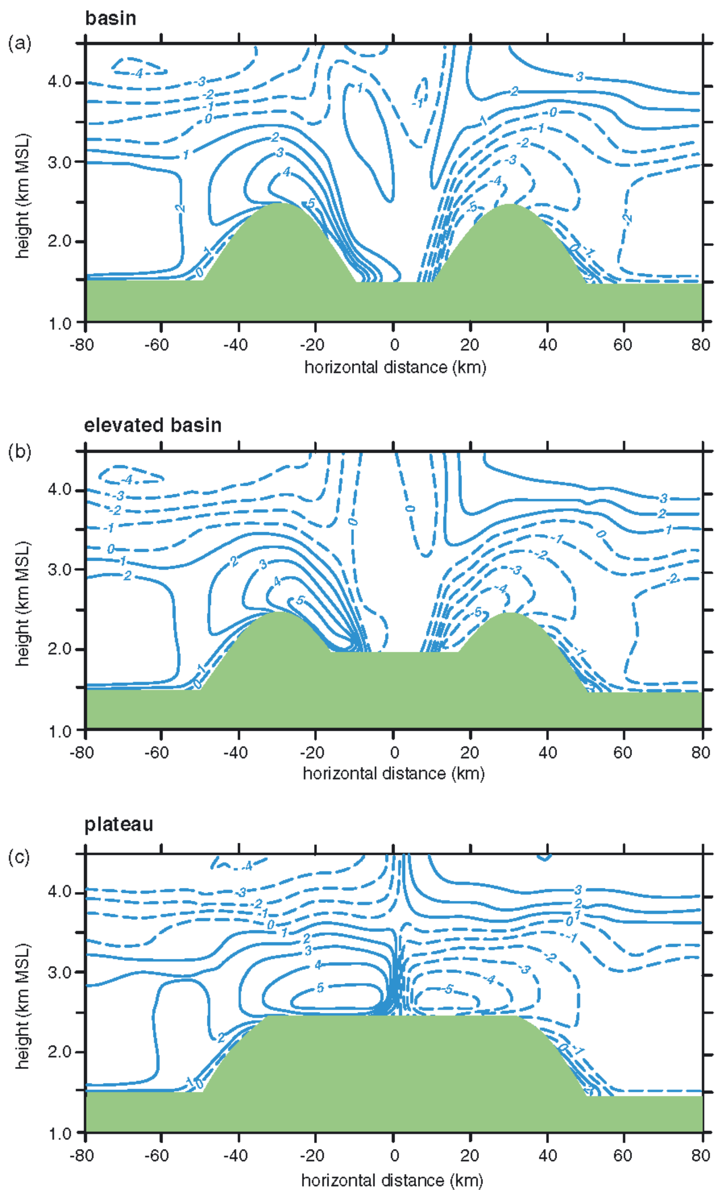

Figure 11.2 The early evening (2000 LST) zonal wind component (m s^{-1}) in a suite of idealized, two-dimensional numerical simulations involving diurnally varying radiative forcing, simple topography, and no ambient wind. In addition to obvious downslope winds, there are larger-scale winds that have also been thermally forced by the valley wind generation mechanism. (Adapted from de Wekker *et al.* [1998].)

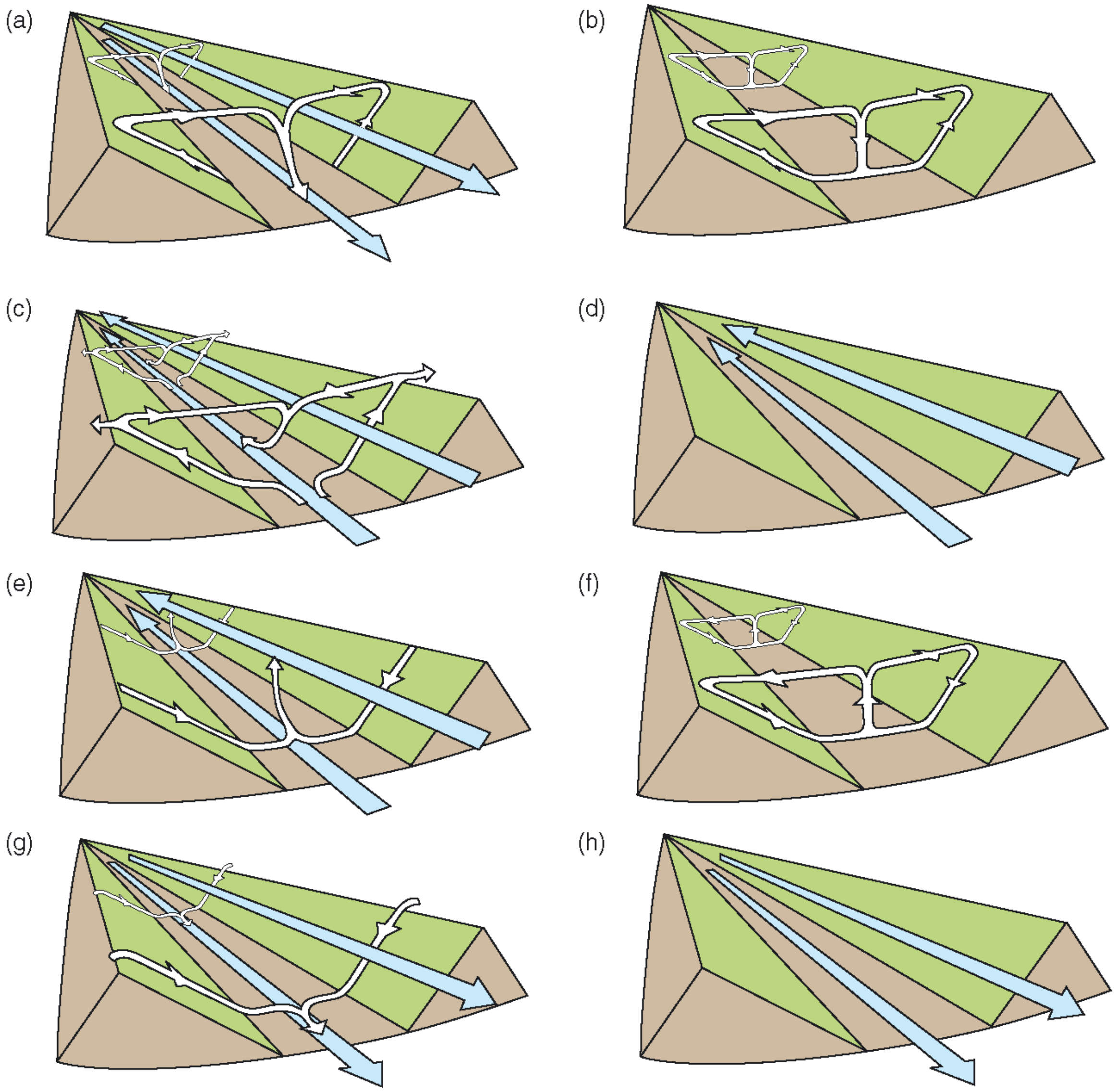

Figure 11.10 Diurnal cycle of valley and slope winds (after Defant [1951]). (a) Sunrise: onset of upslope winds (white arrows) and continuation of downvalley winds (blue arrows) from the previous night. The valley is colder than the plain. (b) Mid-morning (approximately 0900 LST): strong slope winds, transition from downvalley to upvalley wind. The valley is the same temperature as the plain. (c) Noon and early afternoon: diminishing slope winds; fully developed upvalley wind. The valley is warmer than the plain. (d) Late afternoon: slope winds have ceased, the upvalley wind continues. The valley is still warmer than the plain. (e) Evening: onset of downslope winds, diminishing upvalley wind. The valley is slightly warmer than the plain. (f) Early night: well developed downslope winds, transition from upvalley wind to downvalley wind. The valley and plain are at same temperature. (g) Middle of the night: downslope winds continue, the downvalley wind is fully developed. The valley is colder than the plain. (h) Late night to morning: downslope winds have ceased and the downvalley wind fills the valley. The valley is colder than the plain.

July 1981

PROFS

Early morning diurnally forced flow

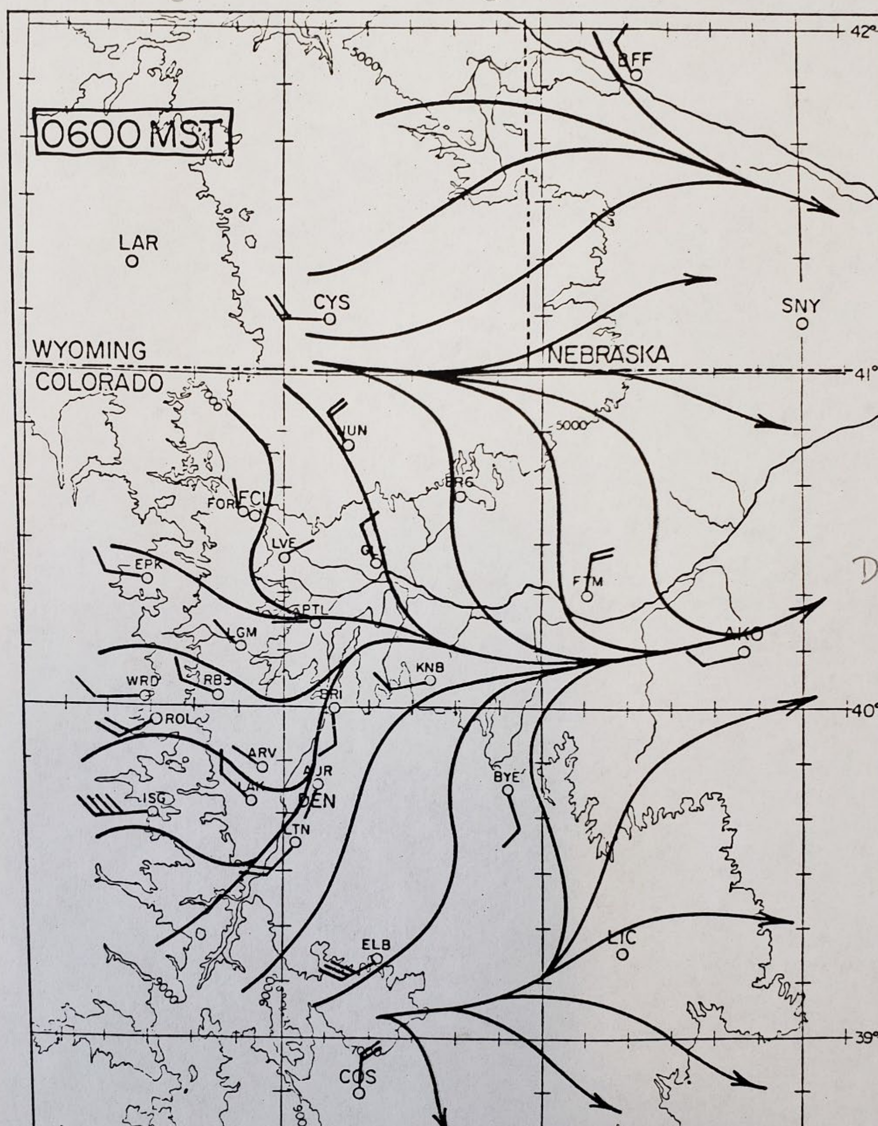

Drainage off ridges to lower river valleys

⌐ = 1kt

Vector average of winds through various days

Johnson and Toth (1982)
Toth + Johnson (1984)
MWR

15 min before sunrise

JOHNSON AND TOTH (1982)

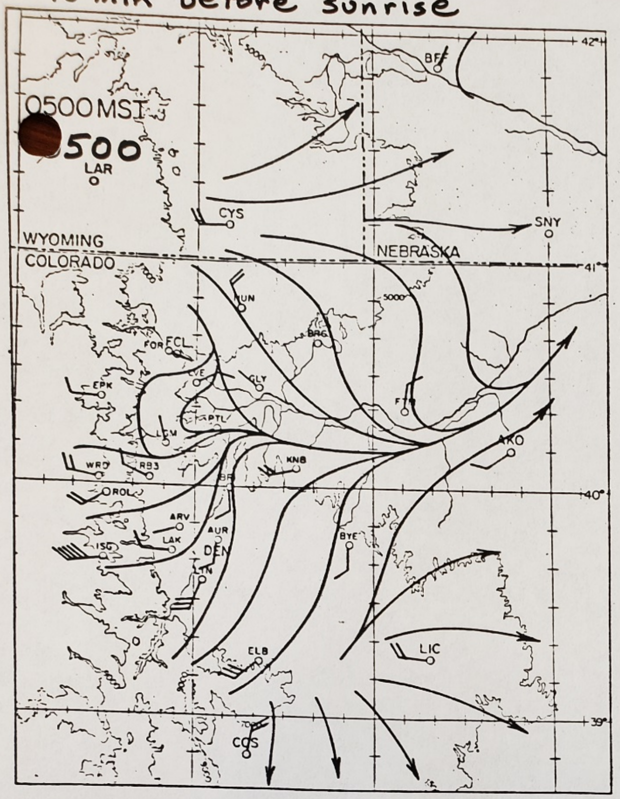

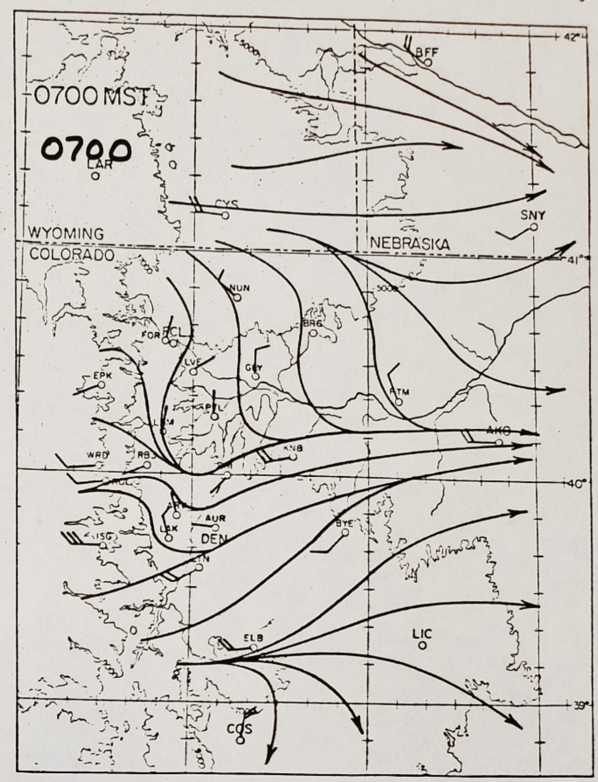

RESULTANT WINDS, JULY 1981 (1 full barb = $1\ m\ s^{-1}$)

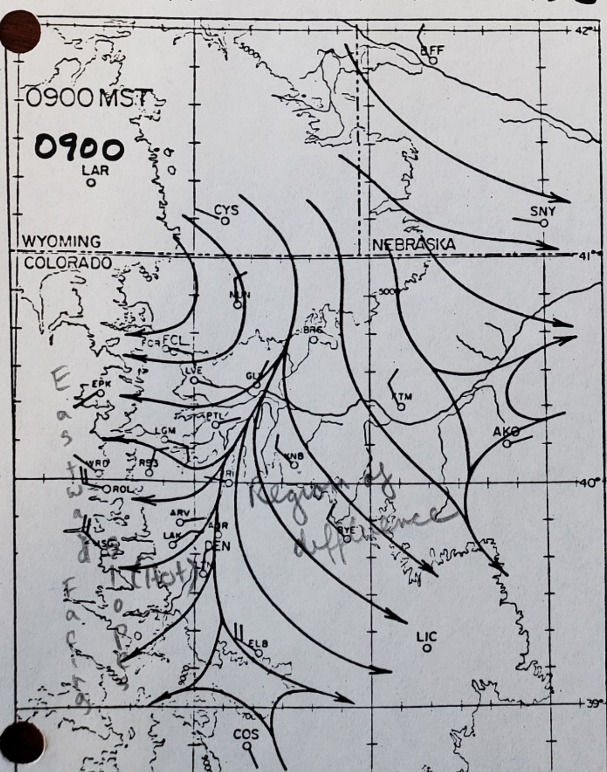

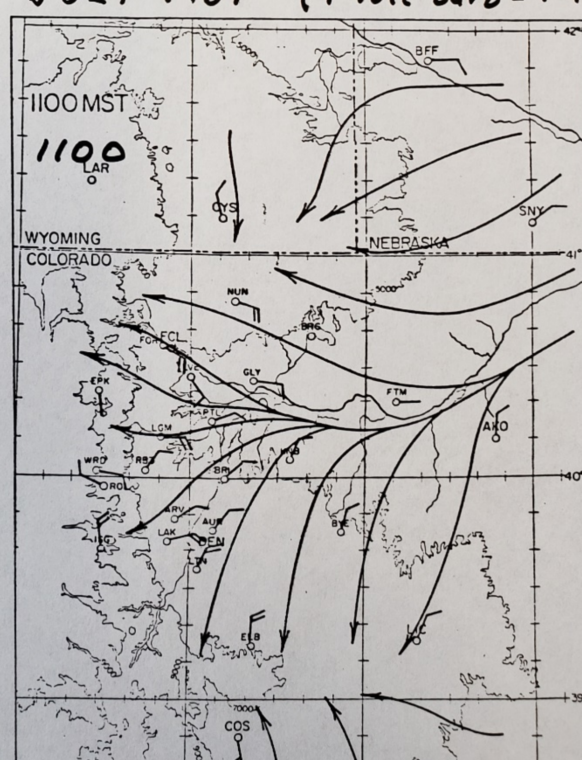

Flow has reversed to upslope along Front Range

Convergent flow on ridges

~100 km

JOHNSON AND TOTH (1982)

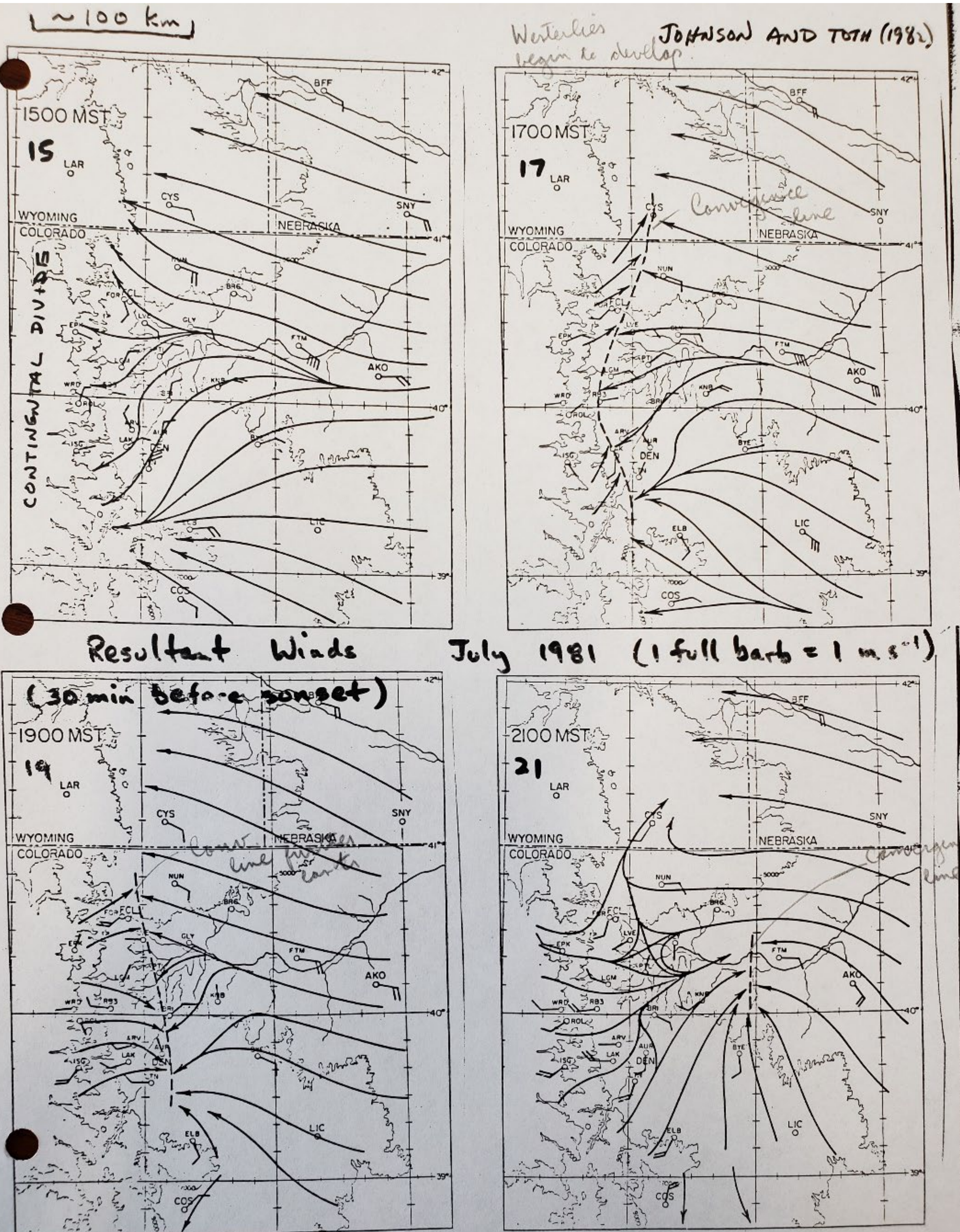

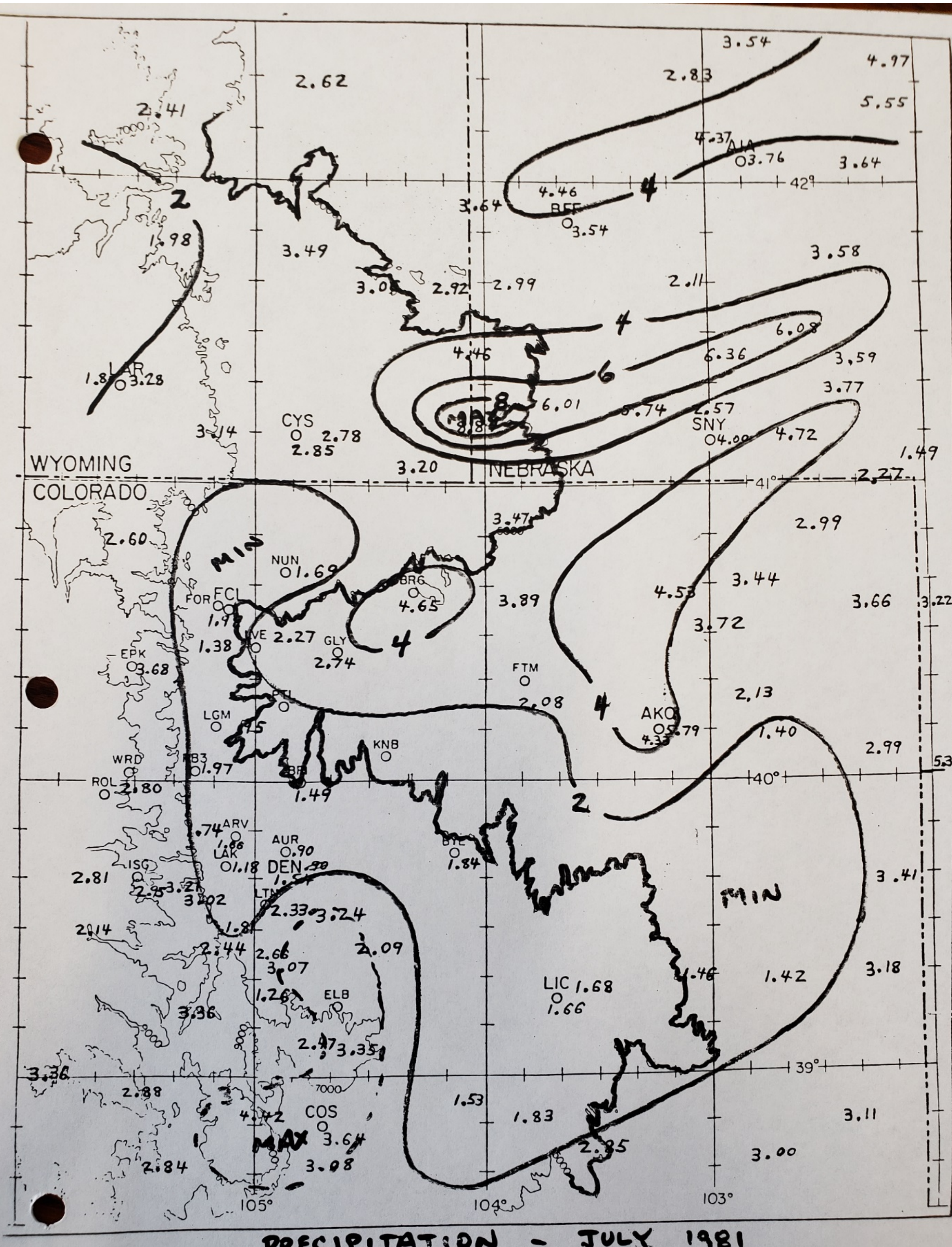

PRECIPITATION - JULY 1981

1100 MST STREAMLINES AND RADAR ECHO FREQUENCY

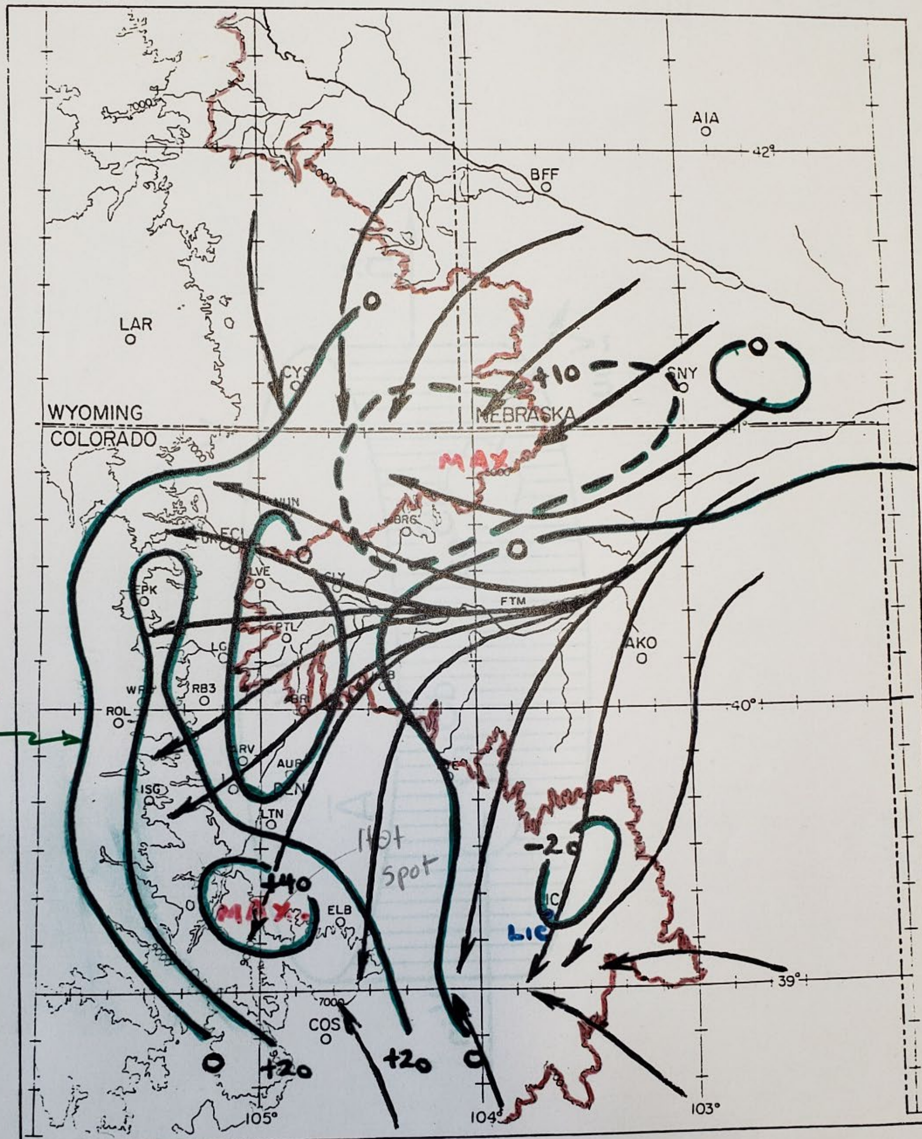

Radar Echo Frequency

(from Wetzel, 1973)

Azimuthally averaged radar echoes from Limon radar. Fig.

PRECIPITATION – JULY NORMAL

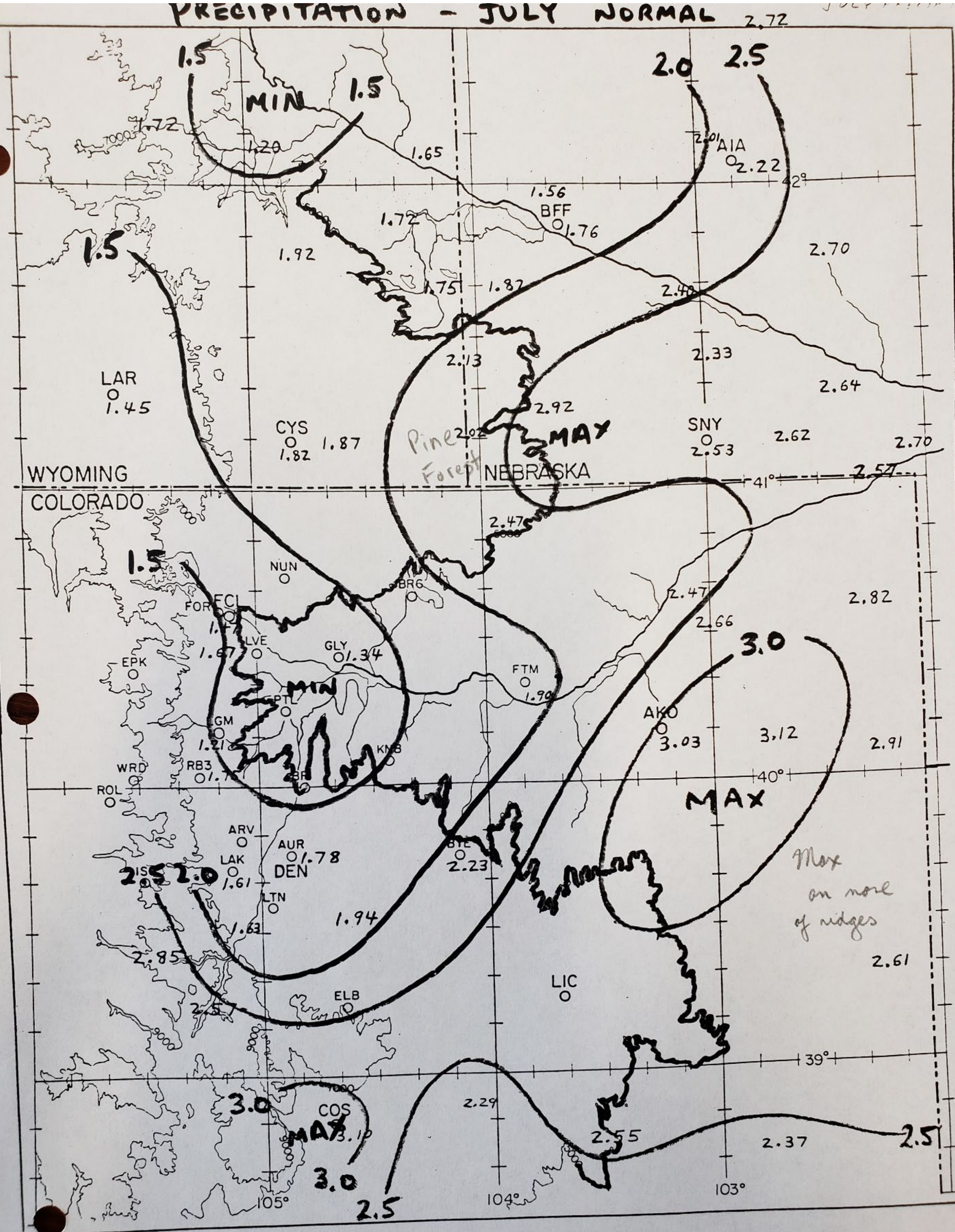

CYCLONIC CIRCULATION INDUCED BY PALMER LAKE DIVIDE (SZOKE et al., 1984) MWR

"DEN CYCLONE"

JUNE 3, 1981

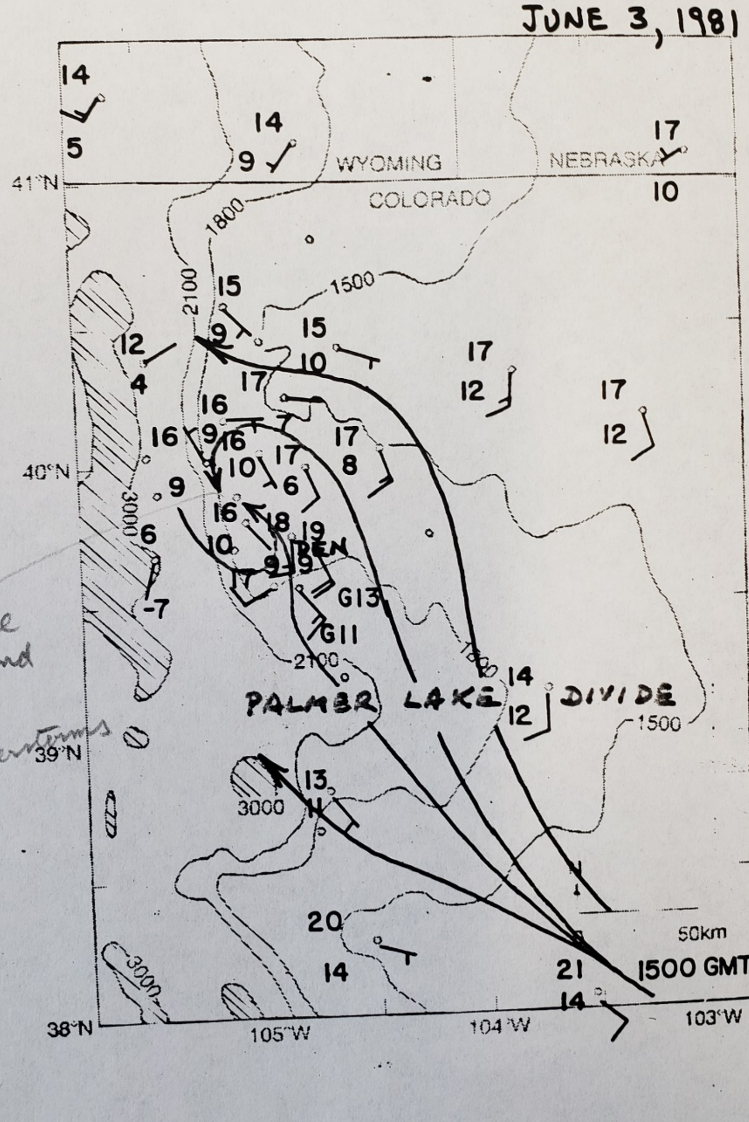

Convergence zone and vorticity → more thunderstorms

Fig 7